Optics Letters

Absolute frequency of cesium $6S_{1/2}$–$6D_{3/2}$ hyperfine transition with a precision to nuclear magnetic octupole interaction

Ting-Ju Chen,[1] Jeng-En Chen,[1] Hsin-Hung Yu,[1] Tz-Wei Liu,[1,2] Ya-Fen Hsiao,[2] Ying-Cheng Chen,[2] Ming-Shien Chang,[2] and Wang-Yau Cheng[1,*]

[1]Department of Physics, National Central University, Taoyuan City 32001, Taiwan
[2]Institute of Atomic and Molecular Science (IAMS), Academia Sinica, Taipei 10617, Taiwan
*Corresponding author: wycheng@phys.ncu.edu.tw

Received 9 February 2018; revised 22 March 2018; accepted 22 March 2018; posted 23 March 2018 (Doc. ID 322908); published 17 April 2018

We have determined the fundamental frequency of the cesium atom $6S_{1/2}$–$6D_{3/2}$ two-photon transition, for the first time, to our knowledge. Moreover, our high-resolution scheme made it possible to address the influence of the nuclear magnetic octupole on the hyperfine structure. We found that the octupole-interaction hyperfine constant deduced from the cesium 6D-level has a value nearly eight times larger than what has been deduced from the 6P-level.

OCIS codes: (120.3940) Metrology; (300.6210) Spectroscopy, atomic; (020.2930) Hyperfine structure.

https://doi.org/10.1364/OL.43.001954

Precisely measuring the frequency of the cesium atom $6S_{1/2}$–$6D_{3/2}$ transition is important for both atomic physics and metrological applications. In atomic physics, knowing the precise valence energy is helpful in high-precision many-body perturbation theory (MBPT) calculations [1]; in metrological applications, determining the frequency of the cesium-stabilized laser is essential for developing a novel optical frequency reference at 885 nm. The significance in the former case is due to the fact that cesium is a high-Z (atomic number) atom; thus, the cesium atom provides the best playground for parity-nonconservation (PNC) experiments [1–4], and theoretical calculations need experimental data for composing accurate basis sets from B-splines approach in MBPT [3]. Moreover, precisely measuring the hyperfine intervals will help to reveal how the nuclear charge distribution influences the cesium valance electron from which we can deduce the nuclear magnetic octupole interaction for comparing with what the nuclear shell model predicted [4]. For metrological applications, the cesium-stabilized 885-nm diode laser could be a convenient and reliable optical frequency reference once the transition frequency has been unveiled; in particular, a hand-sized version frequency-stabilized 885-nm diode laser has been realized [5], while no such secondary standard exists for the wavelengths from 800 nm to 1000 nm [6].

In the past, Ohtsuka *et al.* [7] measured the wavelength of $6D_{3/2}$ hyperfine transitions with non-resonant two-photon spectroscopy, and Kortyna *et al.* [8] measured the hyperfine intervals with the resonant scheme. No experiment has addressed the issue of the "absolute energy level" of cesium $6D_{3/2}$ in the literature, to our knowledge. However, in our previous work [9,10], we were aware that the $6S_{1/2} \rightarrow 8S_{1/2}$ transition frequency determined with a sealed glass cell was not "absolute," since the atmospheric helium might diffuse into glass to cause a blue shift [11]. Therefore, in this report, we prepared an additional cesium cell system, at a background pressure of 10^{-10}-torr ultra-high vacuum (UHV) cell, as an environment to confirm the purity of the commercial cesium cell we have used. The other main feature in this report is that we obtained the hyperfine constants to the precision of the nuclear magnetic octupole interaction. We found that the octupole-interaction hyperfine constant deduced from the cesium 6D-level has a value nearly eight times larger than what has been deduced from the 6P-level [4].

Figure 1 shows the simplified schematic diagram of our experiment where the cesium cell #1 was for stabilizing the master-laser frequency; cesium cell #2, cell #3, and the UHV cell were for resolving the unperturbed $6D_{3/2}$ hyperfine spectrum. All the glass cells were Pyrex cells. The master-laser system in Fig. 1, comprising of a homebuilt extended-cavity diode laser (ECDL) and a tapered amplifier, yielded 500 mW of laser power after two isolators. A small portion of the laser power (20 mW) was used for offset locking, and most of the laser power was split into two optical paths with mutually perpendicular polarizations. Eventually, we achieved 40-mW phase-modulated radiation before entering into cesium cell #1 (Cs #1) and 150-mW unmodulated radiation before entering the same cesium cell from the other side. We used a Rohde &-Schwarz SMB 100A signal generator whose time base referred to a Symmetricom 5071a cesium clock [12], to modulate the electric-optical modulator (EOM, [13]) at an 8470-MHz modulation frequency (Δ), which resulted in a phase modulation of 1.1 radians at the 885-nm wavelength. A 27-kHz sinusoidal modulation was sent into the FM input of the aforementioned signal generator to dither the sidebands that resulted

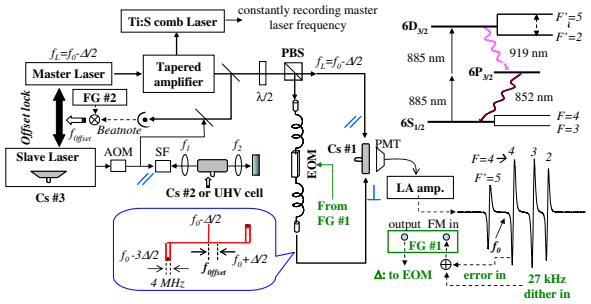

Fig. 1. Simplified block diagram of the experimental setup. LA, lock-in; FG, function generator; Δ: 8470-MHz, 4-MHz sideband dither width (inset); right-bottom: derivative-like "crossover" spectra at 3 ms, see text; f_{offset} offset frequency; SF: spatial filter; UHV cell: high-vacuum cell; $f_{1,2}$: lens with 10 cm focal length.

in a 4-MHz dither-width in the optical frequency. A lock-in amplifier was used to demodulate the 6D-6P-6S fluorescence, which was detected by a photomultiplier tube (PMT). Our PMTs for all cells in this Letter could detect both 919 nm and 852 nm fluorescence. An additional 885-nm interference filter (band reject) was implemented between cell and PMT to keep away the window scattering light caused by laser incidence. The related level diagram of fluorescence can be found in Fig. 1. Consequently, we obtained a derivative-like hyperfine spectrum for laser stabilization with 30 ms time constant, as displayed in the bottom-right of Fig. 1, whereas the relevant level diagram is depicted above the spectrum. The cell wall temperature of Cs #1 was set at 81°C, while that of Cs #3 was set at 53°C to avoid heat-flow-induced convection inside the laser cavity whose temperature was kept at room temperature. The cell wall of Cs #2 was also kept at a similar temperature (53°C). Note that the derivative-like spectrum in Fig. 1 was actually resolved by both the carrier and −1 sideband with the spectrum position at the middle frequency between the carrier and sideband, which was referred to as the "crossover" in reference [14]. When we intend to resolve the spectrum of $6S_{1/2}$ $F = 3 \rightarrow 6D_{3/2}$, $F' = 2$–5 transitions, the crossover frequency of the laser would be pre-stabilized against the $F = 4 \rightarrow F' = 4$ transition frequency (f_0), and the carrier frequency of the master laser (f_{master}) would then be equal to $f_0 - (\Delta/2)$, as indicated in the inset of Fig. 1. The spectrum shown in Fig. 2 was realized by tuning the offset frequency (f_{offset}) in Fig. 1 step by step with the master frequency pre-stabilized. Similarly, we pre-stabilized our master laser to the $F = 3 \rightarrow F' = 5$ transition, as we intended to resolve the spectrum of the $F = 4 \rightarrow F' = 2 - 5$ transitions. We did not change the EOM frequency (Δ), instead of changing the offset frequency (f_{offset}) here, as was performed in reference [9], since the sideband intensity was not exactly constant for the long frequency tuning range in this experiment. The ECDL slave laser in Fig. 1 had an intracavity structure, i.e., we put a cesium cell (Cs #3) inside the laser resonator as was demonstrated in reference [5], except that the previous Fabry–Perot diode was replaced by a high-power AR-coated diode [15]. The output power of the slave laser was 80 mW. After two Faraday isolators (not shown in Fig. 1), we implemented an acousto-optical modulator (AOM) to regulate laser power and, after that, employed a spatial filter to further improve the beam wavefront overlapping [9]. Consequently, 23.6 ± 0.1%-mW of regulated laser power and a well-defined wavefront were presented right before entering Cs #2. We put a Glan–Taylor polarizer to further purify the polarization, which was measured as 10^6 : 1 extinction ratio. The Cs #2 and Cs #3 spectrometers in the slave-laser system actually share the same laser frequency (f_{slave}), which can be expressed as

$$f_{\text{slave}} = f_{\text{master}} + f_{\text{offset}} = f_0 - (\Delta/2) + f_{\text{offset}},$$

and the offset lock reached the level of sub-Hz precision, as was monitored by a frequency counter. Cs #3 had excellent frequency repeatability and yielded a near-natural-linewidth spectrum, due to perfect laser beam overlapping in the cavity and ignorable transit broadening (~130 kHz). However, the compact intracavity structure was inconvenient for studying systematic errors such as the light shift and Zeeman shift. Therefore, we used Cs #2 for studying the spectral features and absolute transition frequency and used a dispenser-based high-vacuum (10^{-10} torr) glass cell (HV cell in Fig. 1) [16] to confirm the measured transition frequency. Only two cells in Fig. 1, namely, Cs #2 and the UHV cell, were wrapped with one layer of mu-metal to reduce the influence of the Earth's magnetic field.

Figure 2 displays a typical Doppler-free two-photon spectroscopy with Voigt fitting (red dashed line), resolved with Cs #2. Note that we did not add Gaussian background in the fitting program. As such, the excellent signal-to-residual ratio in Fig. 2 shows the great advantage of two-photon spectroscopy in terms of removing the Doppler background, which was vital for precisely unveiling the unperturbed Cs *D*-level hyperfine structure. The following three facts led to the highly accurate curve fitting in Fig. 2: first, the optical frequency was simultaneously recorded by a Ti:S comb laser for each data point in Fig. 2, which provided excellent frequency accuracy in the transverse axis. Second, the sampling time of each data

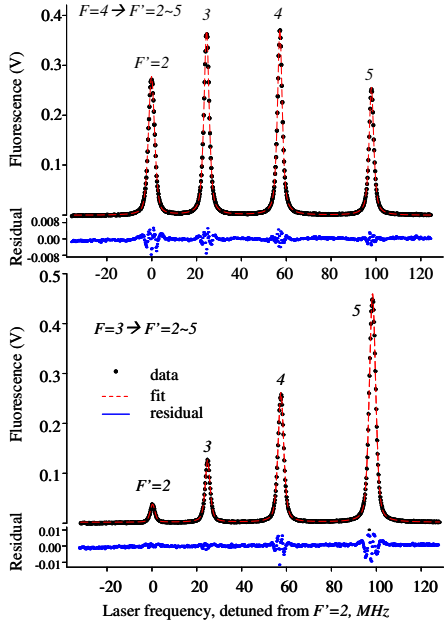

Fig. 2. Cesium $6D_{3/2}$ hyperfine structure (times 2 for real energy intervals). Frequency step for successive dots: 200 kHz; the transverse axis was calibrated with a comb laser (see text).

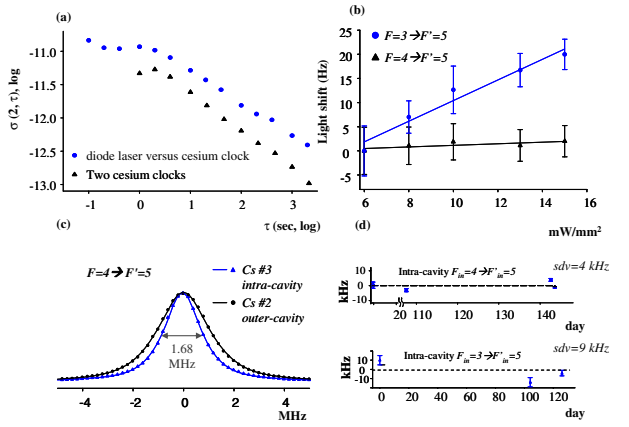

Fig. 3. (a) Two sample Allan deviations $\sigma(2,\tau)$; (b) the largest and smallest light shift. (c) Lineshape resolved by two different cells; (d) frequency repeatability; longitudinal: deviation from the average frequency.

point is 1 s, which efficiently reduced the statistical errors on the signal height. Third, the frequency step between two successive data points was controllable, which offered sufficient data points for the curve fitting. However, owing to the linewidth-limited spectral resolution, a longer sampling time or tiny frequency step would yield no further improvement in terms of the fitting precision. To further improve the accuracy, we averaged six scans on the spectra and determined each transition frequency with an error bar from the six scans. Figure 3 is for investigating the potential of applying our 885-nm frequency-stabilized diode laser as a secondary optical frequency standard. Figure 3(a) is the test of the laser stability, with the laser frequency locked to Cs #1. The Allan deviation was deduced by recording the beatnote between the master laser and one mode of the comb laser, displayed with blue circular dots. Since the repetition rate and offset frequency of our comb laser were all referring to the same cesium clock, the fractional Allan deviation ($\Delta f/f$) was actually a comparison between our frequency-stabilized 885-nm radiation and the cesium clock. The black triangle symbol in Fig. 3(a) is the other Allan deviation of two similar clocks measured before one was sent to our laboratory. We found that the master laser achieved similar frequency stability as that possessed by the cesium atomic beam clock. Figure 3(b) addresses an important issue that was always concerned in the application of two-photon standard [17], i.e., the light shift caused by all intermediate states, and that is inevitable in most two-photon transitions [18]. The good news is that the light shift of the $F = 4 \rightarrow F' = 5$ transition in Fig. 3(b), resolved by Cs #2, is 47 times smaller than that of the cesium 6S-8S transition and more than 1100 times smaller than that in the Rb standard [17]! Unlike what has been found in cesium $6S \rightarrow 8S$ hyperfine transitions [19], a different $6S \rightarrow 6D$ hyperfine level yields a significantly different light shift, as revealed in Fig. 3(b), in which the slope, namely, the frequency shift (mHz) per mw/mm^2 of the $F = 3 \rightarrow F' = 5$ transition, is one order of magnitude larger than that of the $F = 4 \rightarrow F' = 5$ transition. We found that the two transitions have near-zero light shift, as presented in Table 1, i.e., the $F = 3 \rightarrow F' = 4$ and $F = 4 \rightarrow F' = 5$ transitions. This is owing to the fact that the sum of transition amplitudes from the lower level to all intermediate states is coincidentally

Table 1. Features of the Cs $6S_{1/2} \rightarrow 6D_{3/2}$ Transitions

$F = 3 \rightarrow$	$F' = 2$	$F' = 3$	$F' = 4$	$F' = 5$
Light shift[a]	−706 (80)	1150 (149)	128 (154)	2136 (256)
Linewidth[b]	836 (32)	960 (11)	1219 (6)	1232 (3)
Zeeman[c]	4.5 (60)	−3.8 (17)	3.3 (50)	−8.2(16)
$F = 4 \rightarrow$	$F' = 2$	$F' = 3$	$F' = 4$	$F' = 5$
Light shift[a]	420 (55)	1026 (135)	488 (24)	165 (83)
Linewidth[b]	1268 (4)	1064 (3)	880 (3)	840 (4)
Zeeman[c]	2.3 (29)	0.21 (49)	3.1 (13)	−0.60(40)

[a]mHz/(mW/mm^2)); 40 μm waist and area $= 3\pi\omega_0^2/4$ [20].
[b]HWHM, in units of kHz, measured via Cs #3.
[c]In units of kHz/G, at the <1 G regime; measured via Cs #2.

almost equal to the sum of the transition amplitudes from the intermediate states to the upper level, and that causes the cancellation in the two-photon transition [18]. The light shifts in Table 1 are blue shifts except for $F = 3 \rightarrow F' = 2$, which is the other difference from the light shift of the cesium 6S-8S transition (red shift). Figure 3(c) presents two different lineshapes simultaneously resolved with different cesium cells (Cs #2, Cs #3), from which one can easily find that the intracavity cell (Cs #3) yielded much narrower linewidth (blue triangle). All of the Cs #3-based spectra showed similar linewidth shrinking (~750 kHz) compared with those resolved with the Cs #2 system, in spite of the fact that different transitions actually have different measured linewidths. This implies that the "transit time broadening" on the Cs #2 system played an important role in the linewidth discrepancy between the two cells, since the beam waist at the center of Cs #2 was only 40 μm. The linewidth listed in Table 1 comprised the natural linewidth, transit time broadening (~130 kHz in Cs #3), laser linewidth (<100 kHz), Zeeman broadening in μ-metal (not perceived for linear polarization), collision broadening, and power broadening (neither was measureable in our level of precision). We conclude that the linewidths measured by the Cs #3 were near the natural linewidth. Note that our scheme in this Letter resulted in a linewidth resolution improvement by one order of magnitude compared with the previous work [8] in which a scheme of stepwise two-photon absorption was performed.

We wrapped a solenoid coil between the mu-metal and the Cs #2 cell to investigate the Zeeman shift [21], and the results are also presented in Table 1. The overall evaluation from Table 1 suggests that the $F = 4 \rightarrow F' = 2 - 5$ manifold, compared with the $F = 3 \rightarrow F' = 2 - 5$ manifold, was more appropriate to serve as a reliable optical reference as well as to be used for unveiling the $6D_{3/2}$–level hyperfine structure, since they are insensitive to both the light power and the magnetic field. This conclusion can be further supported by Fig. 3(d), which compares the repeatability of the $F = 3 \rightarrow F' = 5$ and $F = 4 \rightarrow F' = 5$ transitions over four months, using the Cs #3 system, where no laser power regulation or magnetic field shielding were performed. The frequency repeatability of the $F = 4 \rightarrow F' = 5$ transition, presented in the upper part of Fig. 3(d), was 4 kHz over the four-month observation period. However, the $F = 3 \rightarrow F' = 5$ frequency repeatability over a 3.5 month observation period was 9 kHz (lower part). Moreover, our previous experiments showed no influence on the hyperfine intervals; even the absolute frequencies were different [9,14].

Table 2. Hyperfine Intervals and Constants at Cs $6D_{3/2}$ Level[a]

	This Work	Kortyna [8]	Ohtsuka [7]
$(f_{45} - f_{44}) * 2$	81.615 (30)	81.8 (1)	81.15 (84)
$(f_{44} - f_{43}) * 2$	65.335 (14)	65.1 (2)	64.18 (51)
$(f_{43} - f_{42}) * 2$	49.164 (24)	49.0 (1)	48.76 (64)
A (MHz)	16.338 (3)	16.34 (3)	16.17 (17)
B (MHz)	−0.136 (24)	−0.1 (2)	0.11 (127)
C (kHz)	4.3 (10)	—	—

[a]Obtained via Cs #3 system (see Fig. 1 and text).

The obtained hyperfine intervals were

$$(f_{45} - f_{44}) * 2 = 5A + \frac{5}{7}B + \frac{40}{7}C = 81.661(13)\ \text{MHz},$$

$$(f_{44} - f_{43}) * 2 = 4A - \frac{2}{7}B - \frac{88}{7}C = 65.336(12)\ \text{MHz},$$

$$(f_{43} - f_{42}) * 2 = 3A - \frac{5}{7}B + \frac{88}{7}C = 48.859(15)\ \text{MHz},$$

where A, B, and C are the related hyperfine constants, and f_{45} stands for the fundamental frequency of the $6S_{1/2}F = 4 - 6D_{3/2}F = 5$ transition, and so on for the others. These hyperfine intervals and the deduced hyperfine constants A, B, and C are shown in Table 2 for a comparison with previous results, which shows that our scheme yielded an improvement by an order of magnitude. The influence of nuclear magnetic octupole moment was hence perceived [4].

The fundamental frequencies of the $6S_{1/2}$, $F = 3$, $4 \rightarrow 6D_{3/2}$, $F = 5'$ two-photon transitions determined via Cs #2 and the UHV cell were

$$\begin{aligned}
&(\text{Cs\#2 } 4\text{–}5'): && 338\ 595\ 897\ 205(14)\ \text{kHz},\\
&(\text{Cs\#2 } 3\text{–}5'): && 338\ 600\ 493\ 509(10)\ \text{kHz},\\
&(\text{UHV cell}, 4\text{–}5'): && 338\ 595\ 897\ 131(96)\ \text{kHz},\\
&(\text{UHV cell}, 3\text{–}5'): && 338\ 600\ 493\ 411(96)\ \text{kHz},
\end{aligned}$$

where all the values have been corrected to zero light and zero magnetic field [9], and the errors are mainly statistical. In particular, the UHV cell yielded larger statistical errors because its signal-to-noise ratio was near one order of magnitude reduced, leading to less repeatability. Nevertheless, the UHV cell offered a clean system that was free from any possible outgassing collision, which was good for confirming the experiments being carried out with commercial cells. For example, we found that the Cs #2 cell yielded the same transition frequency as the UHV cell in the cesium 6S-8S hyperfine transition [11], within our level of measurement precision. Other errors were much smaller than the statistical error, including the light shift correction (2.9 kHz), Zeeman shift correction (1 kHz), pressure shift (<0.5 kHz), misalignment (0.3 kHz), and cesium clock (0.2 kHz), where the approaches of studying the related errors were similar to that in reference [9].

We here presented investigation of the spectral features of the cesium atom $6S_{1/2} \rightarrow 6D_{3/2}$ two-photon transitions and we found that, particularly, the isolated $F = 4 \rightarrow F' = 5$ transition offers a good frequency reference at 885 nm with very low light and Zeeman shifts. Increasing the heating current on the dispenser of the UHV cell would increase the spectrum S/N but led to a short dispenser lifetime. Therefore, we concluded that a sealed cell will be more practical, and it is worthy of thinking about improving cell quality in the next-step experiment to keep away the outgassing or helium diffusion from the atmosphere [9,11]. Our high-precision scheme in this paper also enables us to further determine the hyperfine constant C, while detailed theoretical calculations are desired to deduce the nuclear octupole moment based on our measurement result. It would be very interesting to provide more evidence to resolve the controversy between atomic experiments and the nuclear shell model raised by Gerginov *et al.* [4].

Funding. Ministry of Science and Technology, Taiwan (MOST) (106-2112-M-008-020).

Acknowledgment. We are grateful to Chunghwa Telecommun. Labs, which provided us the cesium atomic clock; Mr. Ya-Po Yang for slave laser structure and electronics with Dr. Chien-Ming Wu; the AMO focus group of Ministry of Science and Technology (MOST) and the CQSE of National Taiwan University, which offered nice platforms for useful communications research.

REFERENCES

1. W. R. Johnson, M. Idrees, and J. Sapirstein, Phys. Rev. A **35**, 3218 (1987).
2. V. A. Dzuba, V. V. Flambaumand, and J. S. M. Ginges, Phys. Rev. A **63**, 062101 (2001).
3. W. R. Johnson, S. A. Blundell, and J. Sapirstein, Phys. Rev. A **37**, 307 (1988).
4. V. Gerginov, A. Derevianko, and C. E. Tanner, Phys. Rev. Lett. **91**, 072501 (2003).
5. Y.-Y. Chen, T.-W. Liu, C.-M. Wu, C.-C. Lee, C.-K. Lee, and W. Y. Cheng, Opt. Lett. **36**, 76 (2011).
6. BIPM, http://www.bipm.org/en/publications/mises-en-pratique/standard-frequencies.html.
7. T. Ohtsuka, N. Nishimiya, T. Fukudaand, and M. Suzuki, J. Phys. Soc. Jpn. **74**, 2487 (2005).
8. A. Kortyna, N. A. Masluk, and T. Bragdon, Phys. Rev. A **74**, 022503 (2006).
9. C.-M. Wu, T.-W. Liu, M.-H. Wu, R.-K. Lee, and W.-Y. Cheng, Opt. Lett. **38**, 3186 (2013).
10. Spotlight on Optics, Optical Society of America, August 2013.
11. W.-Y. Cheng, S. R. Wu, C.-M. Wu, T. W. Liu, and Y. C. Chen, "The influence of atmosphere helium on secondary time standard," in *ICOLS 2017*, Arcachon, Trance, July 2–8, 2017.
12. UTC: Coordinated Universal Time; TL: Telecommunication laboratories of Taiwan.
13. Eospace Inc., "Model: PM-OK5-10-PFU-850-UL-S."
14. C.-M. Wu, T.-W. Liu, and W.-Y. Cheng, Phys. Rev. A **92**, 042504 (2015).
15. Toptica Inc., "Model: LD-0860-0080-AR-2."
16. E. M. Bridge, J. Millen, C. S. Adams, and M. P. A. Jones, Rev. Sci. Instrum. **80**, 013101 (2009).
17. C. S. Edwards, G. P. Barwood, H. S. Margolis, P. Gill, and W. R. C. Rowley, Metrologia **42**, 464 (2005) and reference therein.
18. V. S. Letokhov and V. P. Chebotayev, *Nonlinear Laser Spectroscopy* (Springer-Verlag, 1977), Chap. 4.1.3.
19. C.-Y. Cheng, C.-M. Wu, G.-B. Liao, and W.-Y. Cheng, Opt. Lett. **32**, 563 (2007).
20. B. Girard, G. O. Sitz, R. N. Zare, N. Billy, and J. Vigue, J. Chem. Phys. **97**, 26 (1992).
21. C. Audoin and B. Guinot, *The Measurement of Time* (Cambridge University, 2001), Chap. 6.